Full-scale Testing of Stiffened Extended Shear Tab Connections under Combined Axial and Shear Forces

Mohammad Motallebi[1], Dimitrios G. Lignos[2], Colin A. Rogers[3]

[1] Graduate Research Assistant, Department of Civil Engineering and Applied Mechanics, McGill University, Montreal, QC. Email: mohammad.motallebinasrabadi@mail.mcgill.ca

[2] Dimitrios G. Lignos, Associate Professor, School of Architecture, Civil and Environmental Engineering, Swiss Federal Institute of Technology, Lausanne (EPFL), Lausanne, Switzerland, Email: dimitrios.lignos@epfl.ch

[3] Corresponding author
Colin A. Rogers, Associate Professor, Department of Civil Engineering and Applied Mechanics, McGill University, Montreal, QC. Email: colin.rogers@mcgill.ca
817 Sherbrooke Street West
Montreal QC, Canada, H3A 0C3
Tel. 514 398-6449
Fax. 514 398-7361

ABSTRACT

Owing to the lack of a comprehensive published procedure for the design of stiffened extended shear tabs, practicing engineers usually follow design guides for unstiffened shear tabs. The results of recent laboratory experiments and numerical analyses have demonstrated that improvements to this design approach are warranted. Furthermore, design methods for this connection type under loading scenarios including combined axial and shear forces are not well established. To address these shortcomings, full-scale laboratory tests were carried out on the double-sided configuration of stiffened extended beam-to-girder shear tabs with full depth shear plates. These experiments were complemented by a thoroughly validated finite element (FE) study. Based on the results of these experiments and FE simulations, the connection failure modes were characterized and the axial force along with the other main parameters that affect the connection behaviour were further examined. The current design practice for the double-sided configuration of the full-depth extended beam-to-girder shear tab was also evaluated.

Keywords: extended shear tab, double-sided configuration, gross section yielding, plate out-of-plane deformation, net section fracture

1 Introduction

Shear connections transfer end shear reactions of simply supported beams to supporting columns or girders without transmitting significant flexural moment, i.e. less than 20% of the nominal plastic moment resistance of the supported beam [1]. Furthermore, these connections must have sufficient ductility to sustain rotational demands from a beam's ends. Existing design procedures [2] for shear connections consider only gravity-induced force shear force. However, a simple shear connection may be subjected to an axial force due to wind and/or earthquake while it is resisting gravity-induced shear force. Furthermore, extreme loading scenarios such as the loss of a column develop a significant axial tension in these connections. As a conclusion, contrary to traditional perspectives on simple shear connections, there exists a need for their design under combined axial and shear forces. Despite this need, there is little guidance in the literature for the design of shear connections under combined axial and shear forces [3, 4].

A shear tab is a common type of simple shear connection used in steel construction (Fig. 1). The 15th edition of the AISC steel construction manual [2] considers 89 mm (3.5 in.) as the limit to classify this connection into conventional and extended types based on the distance between the support face and the vertical bolt line closest to the support. Referring to Fig. 1, this is noted as the *a* distance. Extended shear tab connections are considered as a practical and economically attractive solution to join a simply supported beam to a column or girder web. The long plate moves the supported beam clear of the support; as such, there is no need for coping of the beam's flange(s). A common connection configuration is the extended shear tab with a full depth shear plate. In this "stiffened" configuration, the shear plate is shop-welded to the girder web and both flanges (Fig. 1a). In the case of a beam-to-column web connection (Figs. 1b and 1c), the shear plate is welded to the column web and to two stabilizer plates, which in turn are welded to the flanges of the column. Although the stiffened extended shear tab connection is common in steel construction in North America, only a few recommendations [3, 4] have been published for its design. The current AISC design approach for extended shear tabs [2] was originally developed for unstiffened extended shear tabs (Fig. 1d). In this configuration, only the vertical edge of the plate is welded to the support; its horizontal edges are laterally unrestrained.

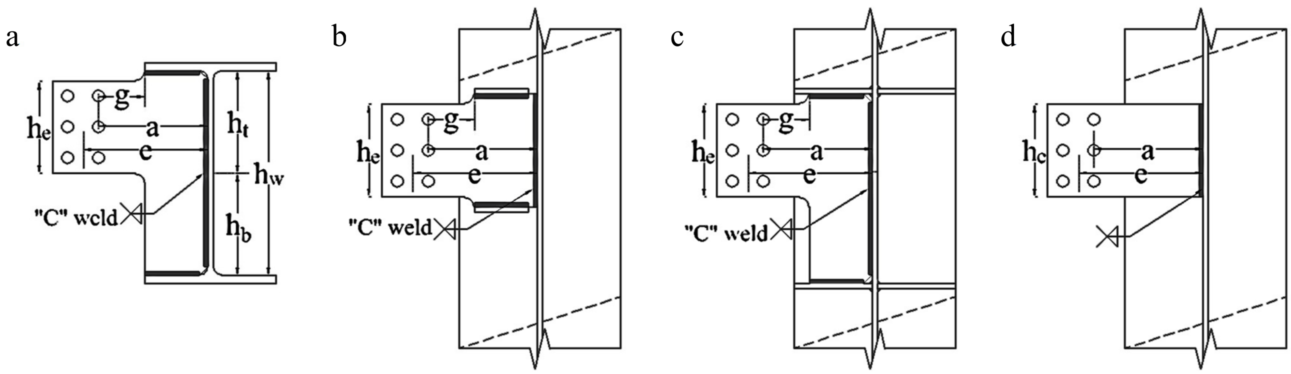

Fig. 1. Single-sided extended shear tab configurations: (a) stiffened beam-to-girder with full-depth shear plate (h_w definition based on CSA-S16 [5]), (b) stiffened beam-to-column, (c) stiffened beam-to-column with continuity plates, (d) unstiffened beam-to-column

Prior studies demonstrated that plate buckling is the governing failure mode for stiffened full-depth configurations of either beam-to-girder [6-10] or beam-to-column shear tab connections [11, 12]. The focus of these research programs was limited to the single-sided configuration of stiffened extended shear tabs. Regarding the behaviour of stiffened extended shear tabs under combined axial and shear forces, Thomas et al. [12] focused on the single-sided configuration, similar to that shown in Fig. 1b. Nevertheless, this configuration would need to be modified if continuity plates were incorporated into a fully restrained beam-to-column connection (Fig. 1c). Thomas et al. [12] determined the shear plate's out-of-plane deformation as the critical failure mode of all ten tests, while the plate completely yielded prior to the connection failure. The range of the applied axial force was limited because the single-sided shear tab experiences small axial force in real world applications due to low stiffness of the girder's weak-axis. In comparison to the single-sided shear tab, the double-sided configuration may be subjected to much higher axial force because the this force transfers through the girder.

This paper presents the results of a coordinated experimental-numerical study aiming to deepen our understanding of the behaviour of the stiffened extended beam-to-girder shear tab under combined axial and shear forces. The testing of full-scale connection specimens allowed for an improved comprehension of the inelastic behaviour of the stiffened extended shear tab, while the test results were relied on to validate the complementary detailed finite element (FE) models. Based on the experimental and numerical results, probable failure modes and their influential parameters were determined. The current design practice was evaluated and recommendations are proposed to improve this design approach for double-sided stiffened extended beam-to-girder shear tab connections with full depth shear plates.

2 Full-scale laboratory testing

Two full-scale connection specimens representing the current design practice in North America were tested in the Jamieson Structures Laboratory at McGill University to examine the behaviour of stiffened extended shear tabs under combined axial and shear forces. These experiments were part of an extensive laboratory testing program [7, 8, 13-18] aiming toward improving the current design and detailing provisions for shear tab connections. The test specimens were chosen to represent the double-sided configuration of a beam-to-girder extended shear tab with full-depth shear plates. The rationale behind choosing the double-sided configuration was its ability to provide a rigid support, allowing the connection to experience a wide range of axial and shear forces. Therefore, the shear-axial force interaction curve could be developed for shear tab's failure modes.

2.1 Description of test specimens

The specimens varied with respect to the number of horizontal bolt lines and the dimensions of the shear plate including its depth, length, and thickness (Fig. 2). The specimen ID, e.g. BG3-2-13-F-200C, identifies the following: BG stands for beam-to-girder configuration, 3 represents the number of horizontal bolt lines, 2 shows the number of vertical bolt lines, 13 demonstrates the thickness of shear plate (mm), F indicates that a full-depth shear plate was used, and 200C represents the magnitude (200 kN) and direction (Compression) of the applied axial force.

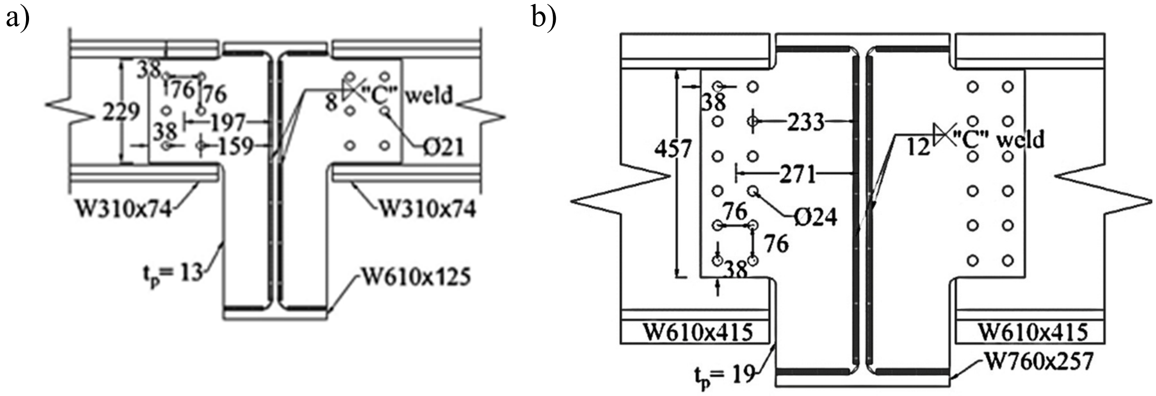

Fig. 2. Double-sided configuration of test specimens: (a) BG3-2-13-F-200C, (b) BG6-2-19-F-500C

In both specimens, the slenderness ratio ($b_f/2t_{pl}$) of the shear plate satisfied the CSA-S16 compactness requirement [5] for plate girder stiffeners ($200/\sqrt{F_y} = 10.7$). However, this is not a requirement for the existing AISC design method because local buckling is not a concern for an unstiffened extended shear tab. Prior studies [7-10] demonstrated the influence of the shear plate compactness on the ductile response of single-sided shear tab connections.

Considering the symmetry of a double-sided shear tab along the girder axis, the laboratory specimens consisted of only half of the connection (Fig. 3), i.e. a single beam connected to a simulated girder. Prior research indicated that the behaviour of single- and double-sided shear tabs is different due to the distortion of the girder web [9]. To simulate one side of the girder two steel plates were joined to the column flange using a complete joint penetration (CJP) weld. The plate dimensions were chosen to be representative of the half width of the girder flange. The shear plate was connected to the girder flanges, as well as to the column flange, through a fillet weld, which was detailed based on the AISC's requirements [2] for the weld of the extended shear tab. The in-plane displacement of the column was restricted using two back braces, which were attached to the strong-floor of the laboratory as described in Section 2.2. These braces, in addition to the strong-axis stiffness of the column, provided a rigid support to the connection being tested and prevented all possible failure modes of the simulated girder.

Furthermore, the bottom flange of both beams was coped to increase the beam-plate gap, and consequently delay beam binding, i.e. contact between the beam's bottom flange and the edge of the shear tab. Preliminary FE analyses suggested that these short copes would not affect the connection global response, although the out-of-plane deformation of the beam and plate might increase slightly.

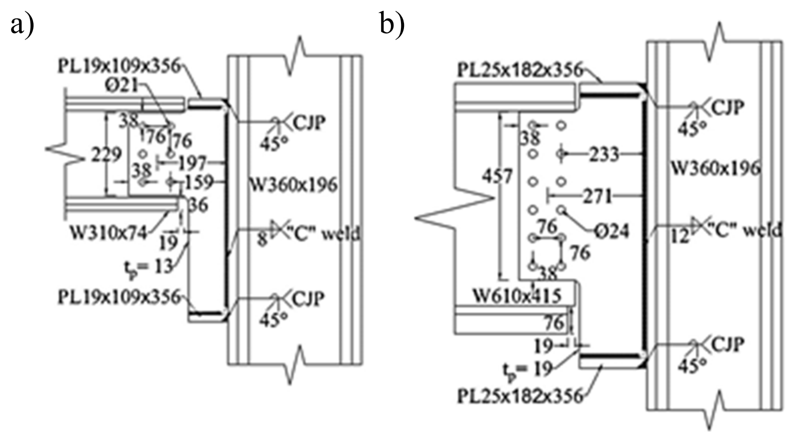

Fig. 3. Details of test specimens: (a) BG3-2-13-F-200C, (b) BG6-2-19-F-500C

The beams and girders were fabricated from ASTM A992 Grade 50 (F_y = 345 MPa) steel [19] while the shear plates were made of ASTM A572 Grade 50 (F_y = 345 MPa) steel [20]. To attach the shear tab to the fabricated supporting girder, an E71T electrode (X_u = 490 MPa) [21] was used in a flux-cored arc welding process with additional shielding gas (CO_2) to provide a fillet weld on both sides of the plate. Each beam was snug tightened to the shear tab using ASTM F3125 Grade A490 bolts [21] in standard size holes, 2mm (1/16”) larger in diameter than the bolts. Figure 4 shows these two specimens prior to testing.

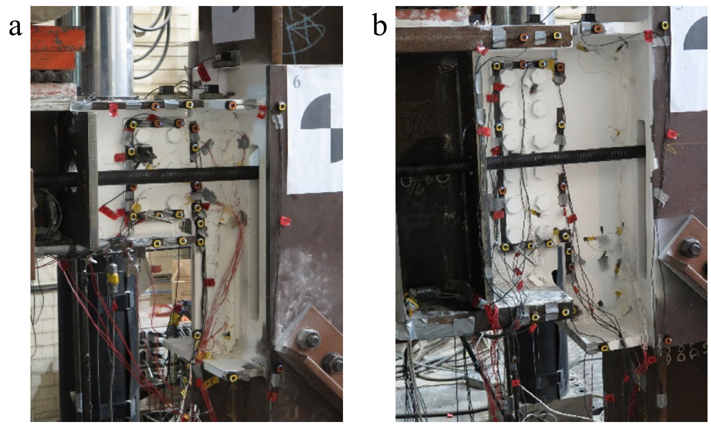

Fig. 4. Specimens: (a) BG3-2-13-F-200C, (b) BG6-2-19-F-500C

Table 1 shows the nominal and expected strength of the connection components along with their measured material properties obtained by ancillary tests in the form of steel and all-weld tensile coupon tests. The test coupons of the shear plates and beams (including web and flanges) were extracted from the same batch of full-scale test components. For each beam, four coupons were cut from the flanges while three were cut from the web. Six coupons were taken from each plate thickness, three along and three perpendicular to the grain direction.

Table 1. Material properties of connection components

Connection components		Nominal		Probable [1]		Measured	
		F_y (MPa)	F_u (MPa)	F_y (MPa)	F_u (MPa)	F_y (MPa)	F_u (MPa)
W310×74	Flange	345	448	379	493	374	490
(W12×50)	Web	345	448	379	493	379	495
W610×415	Flange	345	448	379	493	372	513
(W24×279)	Web	345	448	379	493	377	507
13mm (1/2”) plates		345	448	379	538	432	508
19mm (3/4”) plates		345	448	379	538	377	527
E71T electrode		400	490	--	--	548	620
A490 bolts		896	1034	--	--	--	--

[1] R_yF_y and R_TF_u; for steel plates 1.1 F_y and 1.2 F_u while 1.1 F_y and 1.1 F_u for hot-rolled structural shapes [25]

All steel coupons were tested based on ASTM A370 [22], while two all-weld coupons were tested based on AWS A5.20 [23]. All-weld coupons were extracted from a groove welded assembly of two plates, fabricated from the same weld electrodes used for the shear tab specimens [23, 24]. As neither bolt fracture, nor bolt deformation was observed in these tests, bolt shear tests were not conducted.

The connection specimens were designed based on the current AISC procedure [2] for unstiffened extended shear tabs. This method contains an assumption that the inflection point forms at the support face; the geometric eccentricity (e), distance between the support face and the centre of the bolt group, was chosen as the bolt group eccentricity. As such, the bolt group was designed for the beam end shear reaction (R) and its eccentric bending moment (R × e). The weld line was designed to concentrically resist the beam end reaction (R). To ensure sufficient ductility of the shear tab connection, the weld throat and the plate thickness were detailed such that yielding can develop over the full height of the shear plate's extended portion (h_e in Fig. 1) in advance of bolt shear fracture and weld tearing. The buckling strength of the shear plate was calculated using both the current [7] and previous [26] versions of the AISC design method. To address the higher probability of occurrence of shear plate instability, because of its large eccentricity, the latest AISC design method [2] estimates the shear tab's buckling strength based on the rectangular plate buckling model [1, 27], while its earlier editions [26] used models representative of the flexural buckling of a doubly coped beam [28-30]. To calculate the buckling strength, the distance between the girder web and the interior bolt line (*a* distance) was conservatively chosen to be the unbraced length of the shear plate. Both methods predicted that buckling would not prevent the shear plate from reaching its fully plastic flexural capacity ($M_p=F_yZ_p$). Contrary to the findings from prior research [6-12], the current AISC design method predicted the bolt shear fracture as the connections' governing failure mode.

In addition to the nominal and expected material properties, the measured properties of the steel beam, girder, plate, and weld were used to conduct these AISC-based calculations, whereas the nominal properties of the bolts were relied on in this process. Table 2 contains a summary of the calculated connection strengths corresponding to the probable failure modes. The axial force was not considered in these calculations because the AISC shear tab design procedure is limited to connections that carry shear alone.

Table 2. AISC predicted strength of shear tab test specimens

	BG3-2-13-F			BG6-2-19-F		
Failure mode	Design strength (kN)	Expected strength[1] (kN)	Expected strength[2] (kN)	Design strength (kN)	Expected strength[1] (kN)	Expected strength[3] (kN)
Flexural and shear yielding of shear plate	293	349	391	1088	1278	1251
Shear yielding of shear plate	616	678	761	1835	2018	1976
Bolt bearing	257	377	377	1172	1875	1771
Buckling of shear plate	333	407	456	1351	1651	1616
Rupture at net section of shear plate	430	688	648	1207	1931	1824
Bolt shear	228	337	337	789	1169	1169
Weld tearing	1497	1995	2524	2616	3489	4451

[1]Expected strength based on probable material properties i.e.R_yF_y (1.1 F_y) and R_TF_u (1.2 F_u) for steel plates [25]
[2]Expected strength based on measured material properties i.e F_y=432MPa and F_y=508MPa for 13mm plate
[3]Expected strength based on measured material properties i.e F_y=377MPa and F_y=527MPa for 19mm plate

2.2 Test setup

The test setup (Fig. 5a) consisted of a 12 MN and a 445 kN hydraulic actuator, a lateral bracing system for the steel beam, supporting elements for the connection, and an axial load application system. The 12 MN actuator was located near the shear tab connection and it developed the main shear force in the connection. The 445 kN actuator, placed near the far end of the beam, facilitated the vertical displacement control of the beam tip, as well as the connection rotation. The lateral bracing system was installed to restrict the lateral displacement of the beam, without affecting its vertical displacement. The overall setup has been successfully used in prior research [7, 8, 13-16, 31].

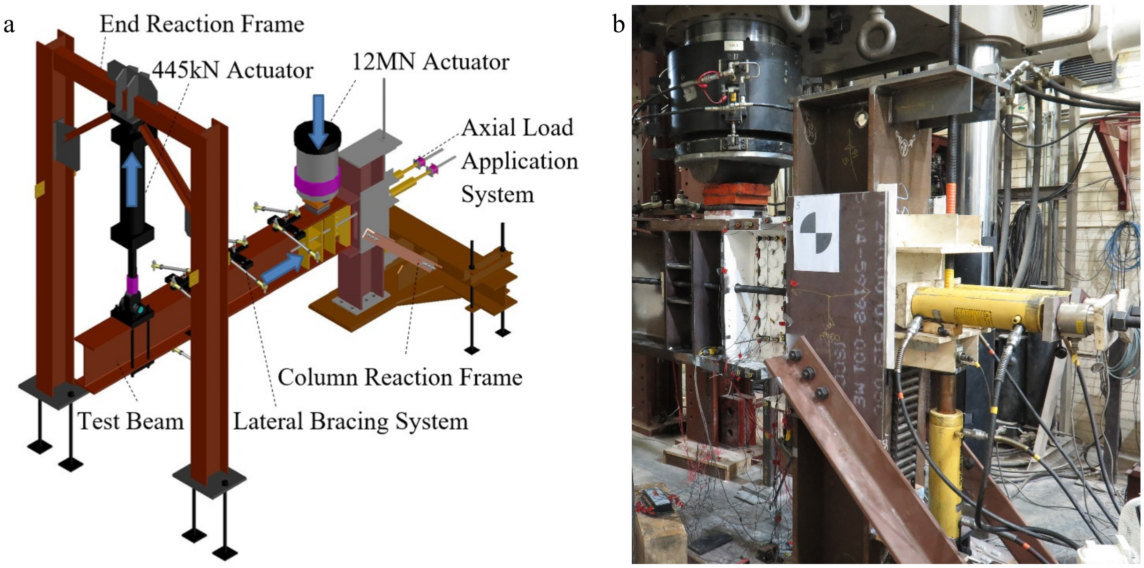

Fig. 5. Laboratory tests: (a) test setup, (b) axial load application system

The axial load application system (Fig. 5b) was used to maintain a constant axial force on the connection, while following the beam end rotation to maintain a force normal to the beam's cross-section. Slots on the column flanges allowed two threaded 31.8 mm (1 ¼") steel rods to pass through and transfer the axial load to a heavily reinforced region of the beam. Further, these rods passed through the moving plate and half cylinder, which allowed for control of the rods' rotation and vertical displacement, respectively. The axial force was generated by two horizontal Enerpac RRH-3010 hydraulic jacks while the vertical displacement of the moving plate was controlled by a vertical 31.8 mm (1 ¼") steel rods pass through an Enerpac cylinder.

2.3 Instrumentation

The implemented test setup was similar to that used in prior research [16], other than the beam lateral bracing system. The new bracing system provided enough free space to implement an optical Coordinate-Measuring Machine (CMM) for 3D measurement of the connection deformation at discrete points (Fig. 6a). Linear Variable Differential Transformers (LVDTs) were installed to measure the shear plate out-of-plane as a backup of the optical CMM system (Fig. 6b).

Inclinometers measured the in-plane rotation of the beam, top girder flange, shear plate, and column. The out-of-plane rotation of the shear plate and beam was measured as well. String potentiometers were used to measure the vertical deformation of the beam and shear plate, as well as the horizontal displacement of the column capping plate. In order to determine the yielding pattern of the connection, it was whitewashed and strain gauges were installed on the shear plate, beam web and flanges adjacent to the connection (Fig. 6c). Load cells were used to monitor the applied vertical and horizontal forces. Vishay Model 5100B scanners and the Vishay System 5000 StrainSmart software were used to record the measured data.

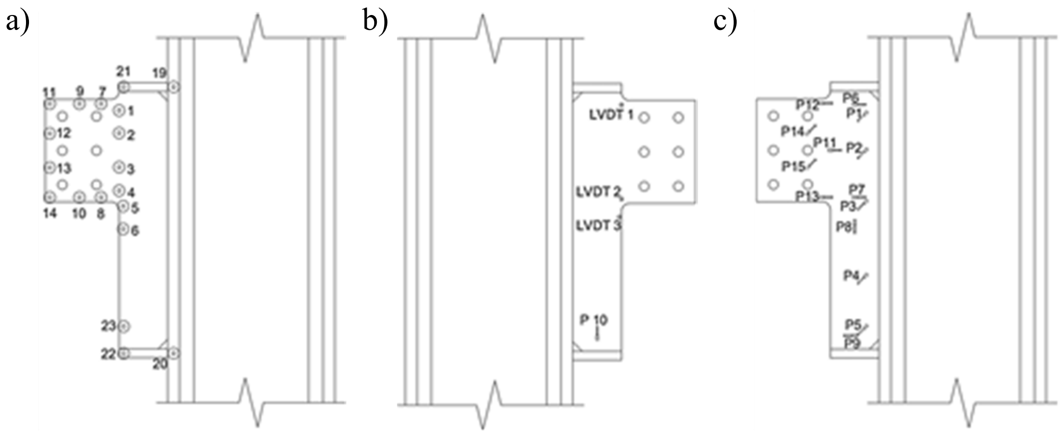

Fig. 6. Instrumentation of Specimen BG3-2-13-F-200C: (a) targets of optical CMM system, (b) LVDTs, (c) strain gauges

2.4 Loading protocol

The loading protocol aimed to simulate end demands of a simply supported beam when subjected to coupled axial and shear force demands. As such, each test specimen was first subjected to its service level of shear load followed by the application of the axial force. From this point in the loading protocol, the axial force was kept constant while the shear demand was increased until failure of the connection. As prior research [16] suggested that shear tab connections locally yielded only in small areas under the service shear load, the axial force was applied in advance of yielding onset based on real time monitoring of strain gauge data. For both specimens, axial force was applied at a connection rotation of approximately 0.0085 rad.

To resemble the rotational demand at the end of a simply supported beam under gravity induced shear force, 0.02 rad relative rotation between the beam and column was set as a target. This was deemed a rational approach based on prior research [31, 32]. This target rotation should be achieved at the connection probable shear resistance, which was calculated based on the expected material properties in lieu of measured ones, as coupons tests could be conducted only after full-scale tests. To follow the loading protocol, the ratio between the displacement rates of the actuators was adjusted constantly up to the target rotation / load point; after reaching this level, the ratio between displacement rates of the actuators was held constant.

2.5 Experimental results

Figure 7 shows the response of both specimens versus the connection rotation, relative rotation between the beam and girder (i.e. the girder top flange). The measured connection shear force was normalized by the shear force corresponding to the plastic shear resistance of the plate's gross section (h_e in Fig. 1), which is equal to 761 kN and 1976 kN for Specimens BG3-2-13-F and BG6-2-19-F, respectively.

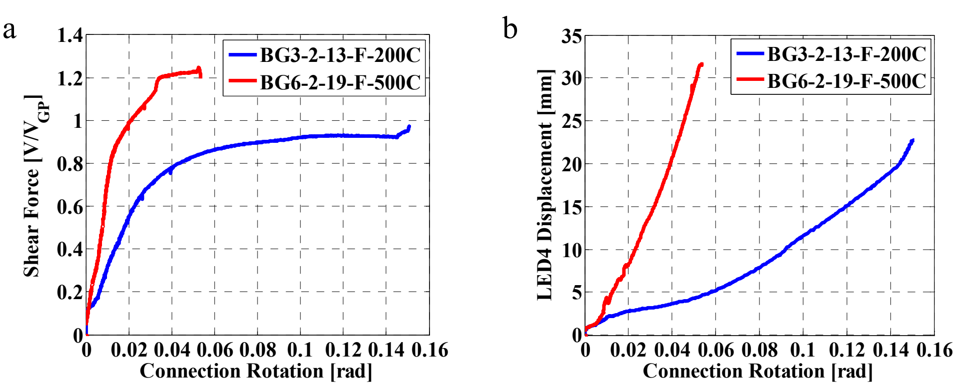

Fig. 7. Measured response vs. connection rotation: (a) connection shear force, (b) shear plate out-of-plane deformation

Referring to Fig. 8a, the axial load was applied to Specimen BG3-2-13-F-200C prior to the plate yielding. The extended portion of the shear plate started to yield along its bottom edge (Strain gauge 13 in Fig 6c) where the compression stress was developed due to the eccentric shear force and the axial compression. Then, plate yielding was observed along the interior bolt line (Strain gauges 14 and 15 in Fig 6c). The top edge of the shear plate yielded after the bottom because the compression force counterbalanced a portion of the developed tensile stress due to the eccentric shear. The connection stiffness reduced at 0.026 rad due to yielding of the extended portion of the shear plate.

The connection shear force still increased and yielding propagated toward the girder web at the stiffener upper portion. Strain gauges P6 and P7 indicated that there was flexural yielding due to the eccentric shear force. The stiffener strain gauges, installed adjacent to the girder web, demonstrated the non-uniform distribution of the shear force along the stiffener. Strain gauges P1, P2, and P3 reported yielding stress, while the recorded shear strain of strain gauges P4 and P5 was negligible. The connection stiffness decreased again when the slope of the curve representing the out-of-plane deformation of the plate bottom edge (LED4, Fig. 6a) largely increased. The connection shear force still increased, while the out-of-plane deformation of the plate increased. Following a shear strength plateau (Figs.8b and 8c), binding between the shear plate and the bottom edge of the beam web slightly increased the shear resistance of Specimen BG3-2-13-F-200C. The test was terminated when the beam's bottom flange started to bind on the shear plate (Fig. 9a). The out-of-plane deformation of the shear plate was obvious at the end of the test (Figs. 9b-9d). The tested specimens responded similarly to the combined axial and shear forces other than the strength plateau, which was precluded by binding in Specimen BG6-2-19-F-500.

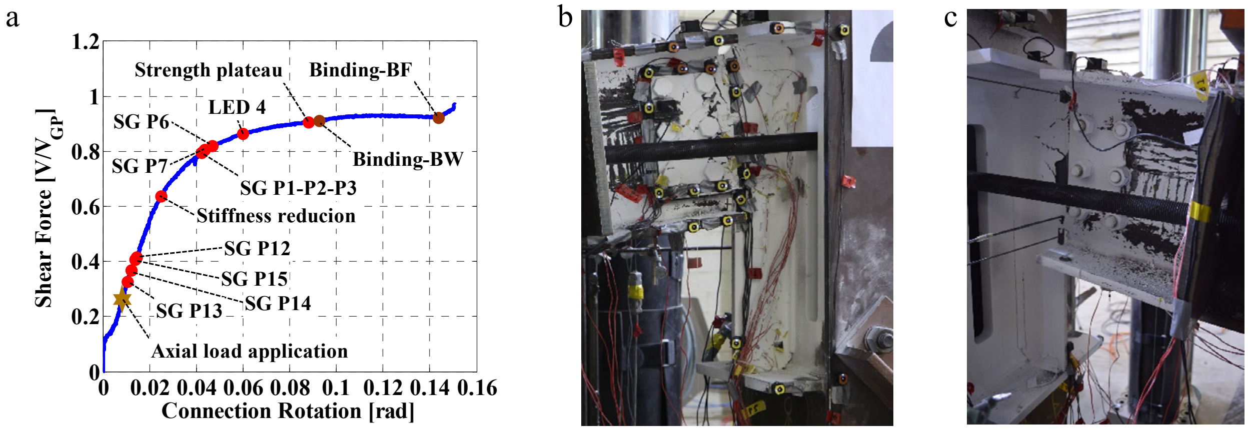

Fig. 8. Specimen BG3-2-13-F-200C: (a) damage propagation, (b and c) deformed shape at strength plataeu

Through post-test examination, bolt bearing was obvious along the interior vertical bolt line of both shear plates. Referring to Fig. 10, the bearing deformation was larger at the upper portion of the plate where the tensile and shear stress developed simultaneously due to the applied bending moment and shear force, respectively. In comparison to Specimen BG6-2-19-F (Fig. 11), small fractures and larger bearing deformation were observed along the interior bolt holes in Specimen BG3-2-13-F (Figs. 10). After unloading the specimens, a diagonal crack was observed at the bottom re-entrant corner of the shear plate (Figs. 10c and 11c). It is believed that this occurred due to the out-of-plane deformation of the shear plate and binding between the beam web and the shear plate.

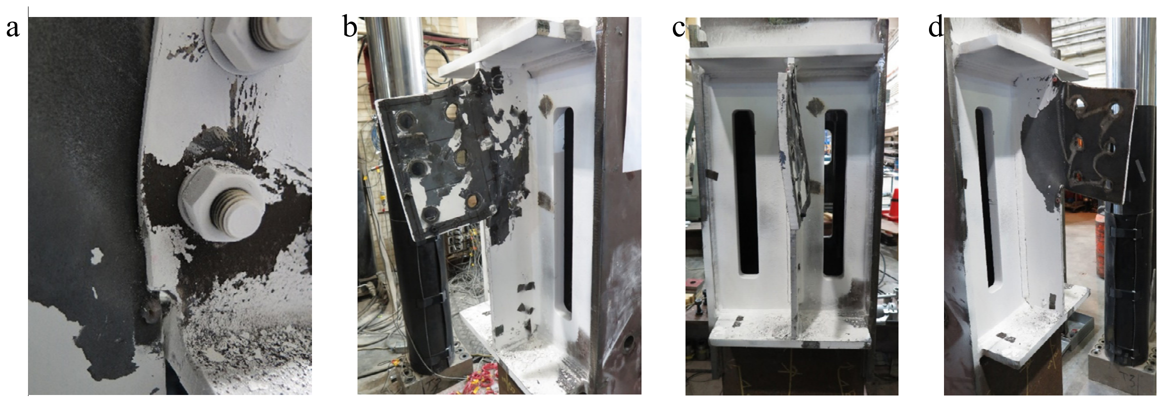

Fig. 9. Specimen BG3-2-13-F-200 : (a) binding between beam flange and shear plate, (b-d) deformed shape at end of test

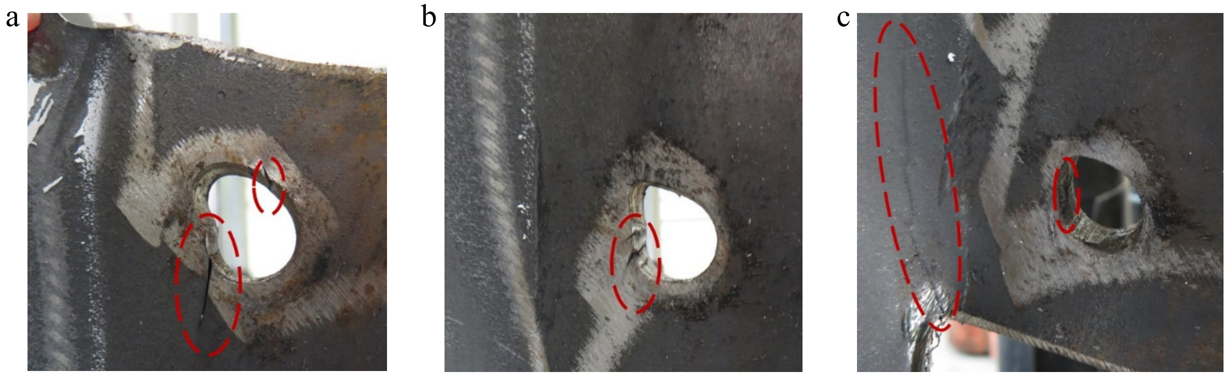

Fig. 10. Bearing deformation and fracture along the interior bolt line of specimen BG3-2-13-F-200C at: (a) top bolt hole, (b) middle bolt hole, (c) bottom bolt hole

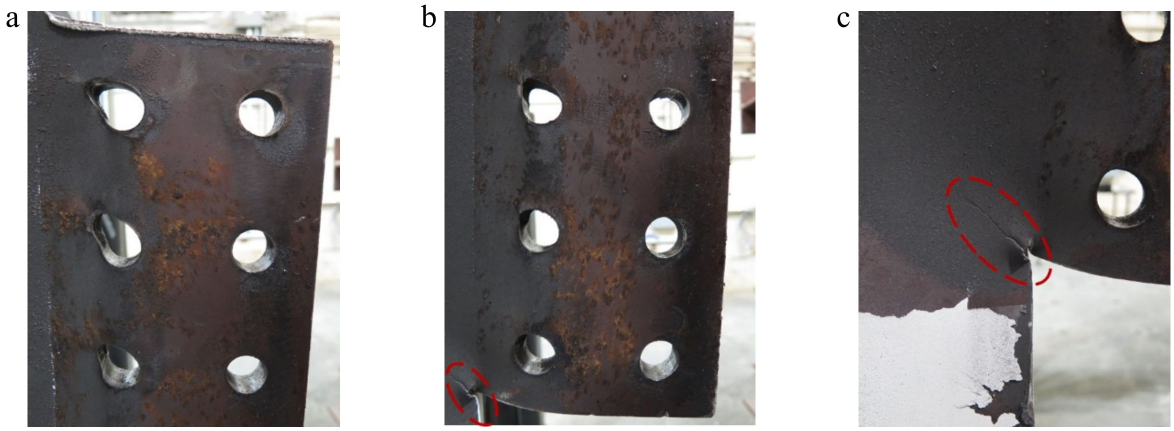

Fig. 11. Specimen BG6-2-19-F-500C: (a) bolt bearing at plate top half, (b) bolt bearing at plate bottom half, (c) diagonal crack at bottom re-entrant corner

To evaluate the accuracy of the current design procedure for extended shear tab connections **, its predictions were compared with laboratory test observations. Referring to Table 2, the current design method suggests that bolt shear fracture should be the governing failure mode. However bolt fracture was not observed in the laboratory tests. Furthermore, no evidence of bolt deformation was observed through post-test examination. The connection stiffness started to decrease at a shear force, which was much larger than the expected resistance corresponding to the flexural and shear yielding of the shear plate. These discrepancies were due to the current design method assumption that the inflection point formed at the support face; hence, the design strength was calculated based on the geometric eccentricity.

The out-of-plane deformation of the shear plate started to increase rapidly when yielding propagated into the stiffened portion of the plate, which resulted in a reduction of the connection strength. This deformation would likely have been more severe if the shear plate had not satisfied the CSA-S16 compactness requirements [5] for the plate girder stiffeners. Of note, the observed out-of-plane deformation was the result of the combined compression and flexural moment of the shear tab, as demonstrated later on in subsequent FE analyses (Section 3).

In addition to the plate yielding, the bolt bearing contributed to the connection ductility. Although the bearing deformation was quite large along the interior vertical bolt line of the shear plate, bearing failure was not considered to have occurred based on observations. The connection shear force became larger than the predicted strength corresponding to the net section fracture, while minor tearing around the bolt holes were observed only in Specimen BG3-2-13-F-200C. This could be attributed to the compressive force influence and the inherent conservatism of the design equation for net section fracture. Furthermore, it was not possible to determine the connections' ultimate failure mode because binding between the beam web and shear plate changed the load transfer mechanism at the end of the test. The ultimate failure mode could, however, be determined through finite element simulations by excluding the beam binding (Section 3).

3 Complementary finite element simulations

Complementary finite element (FE) simulations were conducted to further understand the load transfer mechanism in stiffened extended shear tab connections subjected to coupled gravity and axial loads. Several parameters were interrogated that were not evaluated through experiments, including the axial force and the connection's ultimate failure mode. The FE models were developed in the commercial software ABAQUS-6.11-3 [33]. The features of the FE models were chosen to be representative of those seen in the laboratory experiments; including geometry, boundary conditions, material properties, element size and element type, contacts and interactions, and the imposed loading protocol [9, 10]. The employed material properties were defined based on true stress-strain curves of the various components shown in Fig. 12. Other than the bolt's characteristic response, the implemented stress-strain curves were obtained from testing of the tensile coupons. The bolt's material properties were defined based on typical stress-strain curves reported in Kulak et al. [34], which were scaled to meet the minimum specified values for ASTM F3125 Grade A490 bolts [21].

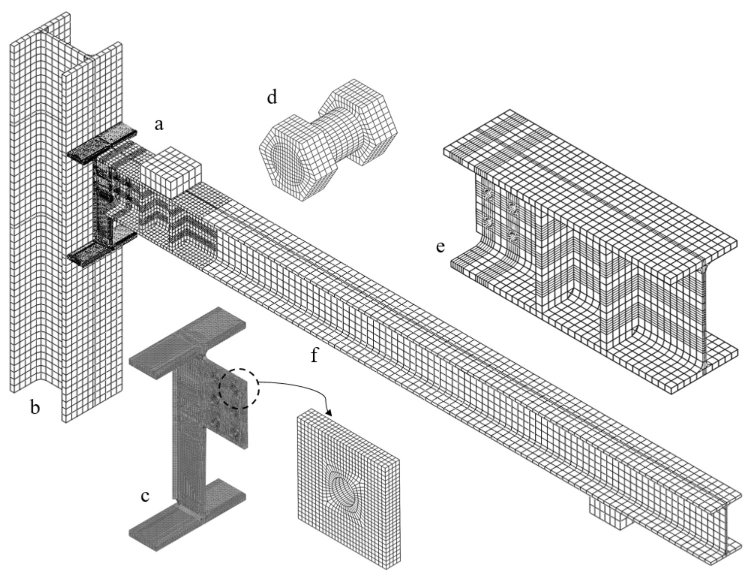

Fig. 12. Finite element model specifics: (a) overall model, (b) column mesh (typical element size of 40 mm), (c) shear plate mesh (typical element size of 3 mm), (d) bolt mesh (typical element size of 1.5 mm), (e) mesh of the beam in the vicinity of connection (typical element size of 20 mm), (f) beam mesh (typical element size of 40 mm)

First-order fully-integrated 3D solid elements (C3D8) were utilized to mesh the components. Based on a mesh refinement analysis, the element size (Fig. 11) was determined. Frictionless interaction was defined for surface-to-surface contact pairs between the load cubes and the beam flanges. For all other components in contact, surface-to-surface contact pairs with a friction coefficient of 0.3 was used to allow transmission of tangential force. Furthermore, possible local instabilities of the shear tab connection were triggered by the introduction of local imperfections into the shear plate. These local imperfections were proportioned to the limits of manufacturing tolerances for the web and flange of W-sections [35-37]. This approach has been successfully implemented in prior FE studies concerned with member and local instabilities [38].

3.1 Model validation

To evaluate the accuracy of the numerical analyses, the FE model predictions were compared with the experimental measurements. The developed connection shear force and the out-of-plane deformation of the shear plate were chosen as the FE model verification criteria.

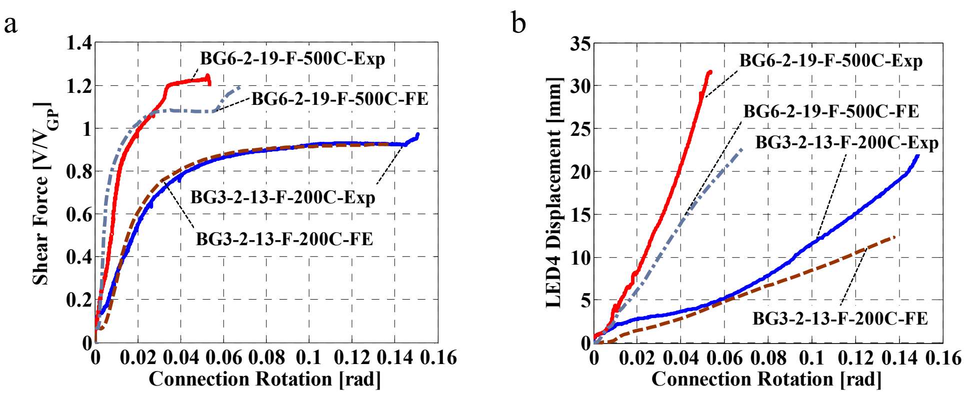

Fig. 13. FE model verification: (a) shear force, (b) shear plate out-of-plane deformation

Referring to Fig. 13, the FE model predicted reasonably well the connection response up to the point where the beam web started bearing on the stiffened portion of the shear plate. This discrepancy was due to the uncertainties related to the contact between beam web bottom edge and the shear plate. In addition to the fabrication tolerance and installation of the respective test specimens, these uncertainties arise because of the imperfections introduced into the FE model. The applied imperfections were an estimate based on the connection bifurcation buckling and allowable manufacturing tolerance of W sections. Of note, structural engineers typically neglect the over-strength in a connection due to beam binding because it is neither desirable nor dependable.

As a snug-tightened connection, the initial response of a shear tab connection depended greatly on the contact between shanks of the bolts and the bolt holes. Because the initial position of each bolt in its hole could not be controlled in the laboratory tests, the bolts were placed at the centre of the bolt hole in the FE model, resulting in a 1 mm (1/32 in.) gap around the entire perimeter. Therefore, the real contact conditions of the bolts may be different from those assumed in the FE models. Due to this discrepancy, the FE model predictions for the connection shear force deviated from the test measurements in the initial increments of the applied loading.

3.2 Simulation results

Figures 14 and 15 show the normalized predictions of the FE models. Referring to Figs. 14a and 15a, the shear force along the outer end of the shear plate re-entrant corners was normalized based on the plastic shear resistance of the gross section ($V_{GP} = 0.6F_yA_g$), while the plate's plastic shear resistance of the net section ($V_{NP} = 0.6F_yA_{net}$) was implemented to normalize the shear force along the bolt line (Figs. 14b and 15b). The plastic bending moment resistance of the gross section ($M_{GP} = F_yZ_g$) was used to normalize the bending moment at the plate's gross section, as shown in Figs. 14c and 15c. The bending moment along the plate's interior bolt line (Figs. 14d and 15d) was normalized based on the flexural capacity of the plate's net section ($M_{NP} = F_yZ_{net}$). The plastic section modulus was defined for an odd number of horizontal bolt lines as $Z_{net} = 1/4t_{pl}(s-d_h)(n^2s+d_h)$, while $Z_{net} = 1/4t_{pl}(s-d_h)(n^2s)$ was used for an even number of horizontal bolt lines [39]. In these equations, n=number of horizontal bolt lines, s=bolt spacing, d_h=diameter of bolt hole, t_{pl}=plate thickness, and d_{pl}=plate depth. The aforementioned plastic capacities of the shear plate, shown in Table 3, were calculated based on its measured dimensions and yield stress.

Table 3. Calculated plastic capacities of shear tab test specimens

Specimens	BG3-2-13-F	BG6-2-19-F
P_{GP} $(F_y A_g = F_y d_{pl} t_{pl})$	1268 kN	3294 kN
P_{NP} $(F_y A_{net} = F_y (d_{pl} - nd_h) t_{pl})$	950 kN	2331 kN
V_{GP} $(0.6F_y A_g = 0.6F_y d_{pl} t_{pl})$	761 kN	1976 kN
V_{NP} $(0.6F_y A_{net} = 0.6F_y (d_{pl} - nd_h) t_{pl})$	570 kN	1398 kN
M_{GP} $(F_y Z_g = F_y t_{pl} d_{pl}^2/4)$	72.5 kN.m	376.5 kN.m
M_{NP} $(F_y Z_{net})$	54.0 kN.m	256.8 kN.m

Regarding Specimen BG3-2-10-F, a comparison between the normalized shear flow and the connection rotation (Figs. 14a and 14b) demonstrated that only a fraction of the connection shear force was transferred through the net section along the centerline of the bolt holes, the critical section with the smallest cross-sectional area along the plate. Referring to Fig. 14a, Specimen BG3-2-13-F experienced the connection shear force equal to 614 kN (V/V_{GP} =0.81) at 0.04 rad rotation while the net section was subjected to only 463 kN shear force (V_N/V_{NP} =0.81 in Fig. 14b). Figures 15a and 15b show a similar trend for Specimen BG6-2-19-F. This observation, which coincided with prior research studies [40], was due to the bearing mechanism between the bolt shanks and the bolt holes. This is further elaborated in Section 4.2. A larger bending moment developed at the gross section (Figs. 14c and 15c) in comparison to the net section (Figs. 14d and 15d) because the inflection point (Figs. 14e and 15e) formed far from the column face, farther from the bolt group centroid.

To evaluate the influence of the axial load on the observed connection behaviour and failure modes, additional FE analyses were carried out for each specimen. Only gravity-induced shear force was applied to the connection in the first FE analysis, while the connection was subjected to combined tensile and shear forces in the second one. These FE models were subjected to the representative experiment loading protocols; to maintain simplicity, the magnitude of the tensile force in the analysis was set equal to the magnitude of the compression force used during testing.

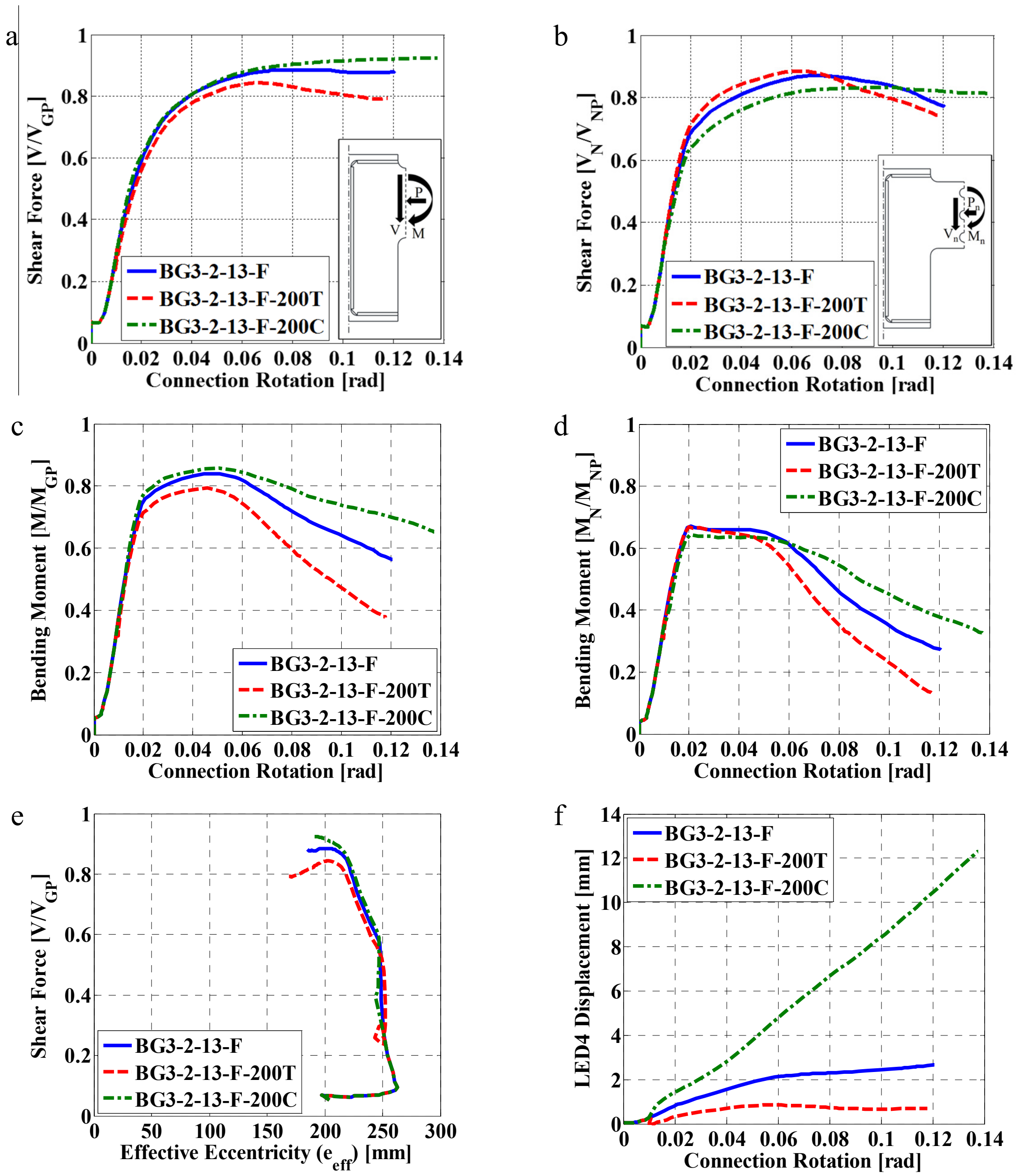

Fig. 14. Simulated response of Specimen BG3-2-13-F: (a) connection shear force, (b) net section shear force, (c)gross section bending moment, (d) net section bending moment, (e) effective eccentricity, (f) plate out-of-plane deformation

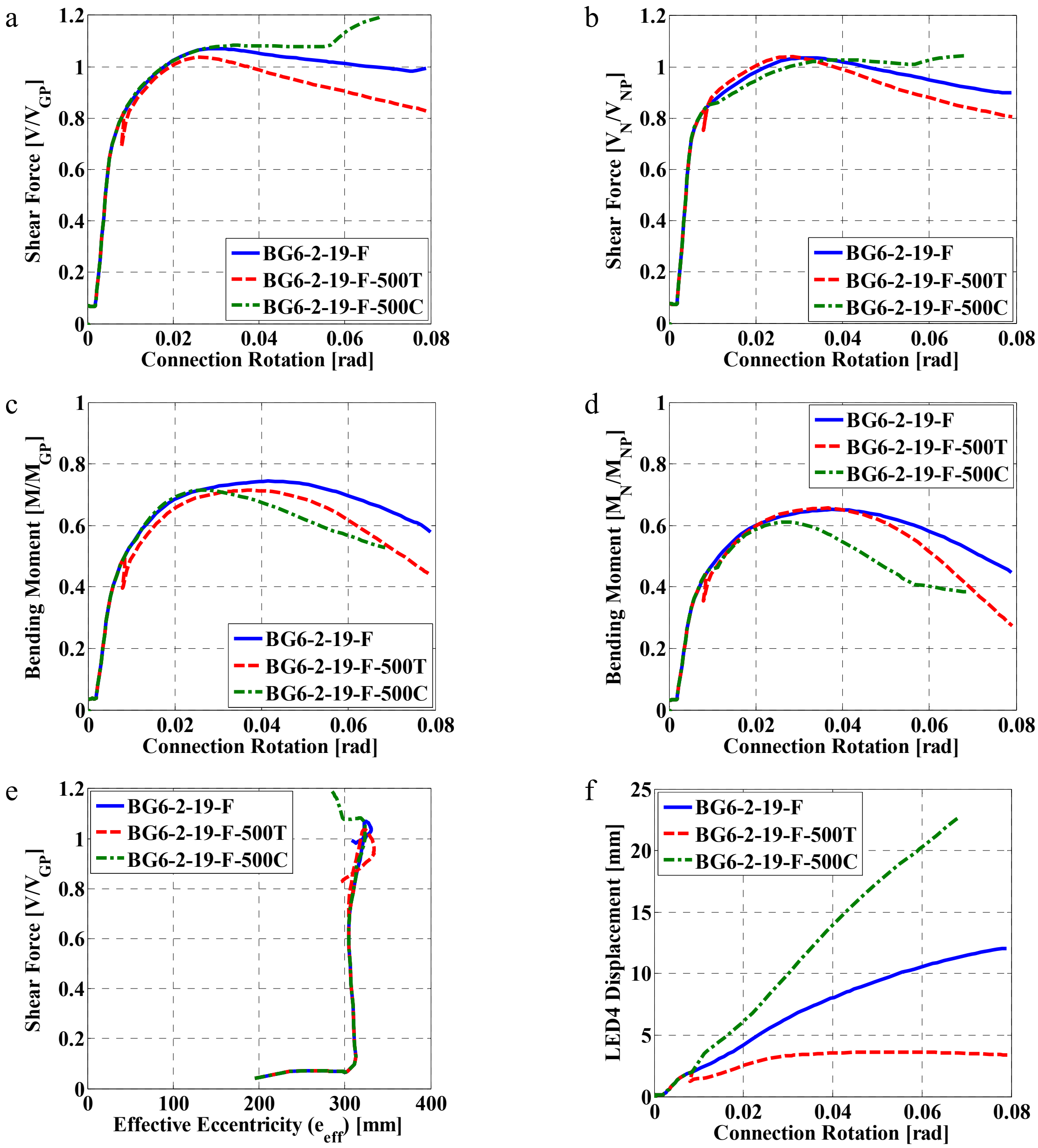

Fig. 15. Simulated response of Specimen BG6-2-19-F: (a) connection shear force, (b) net section shear force, (c)gross section bending moment, (d) net section bending moment, (e) effective eccentricity, (f) plate out-of-plane deformation

In all FE models, gross and net section yielding of the shear plate were observed and the net section fracture along the plate interior bolt line was determined as the connection's ultimate failure mode. Referring to Figs. 14 and 15, the axial force affected the connection's response slightly because the level of the applied axial load was small (P/P_{GY}=0.16 and 0.15 for Specimens BG3-2-13-F and BG6-2-19-F, respectively).

4 Discussion

4.1 Shear plate yielding

Referring to Fig. 16, Neal's interaction equation [41] was used to account for the interaction of axial, shear, and flexural loads at the plate gross and net sections. It was observed that the results of Neal's [41] and the AISC's [2] interaction equations (Eqs. 1 and 2, respectively) were almost equal. Of note, Astaneh proposed Eq. (2) as a simplified version of Neal's interaction equation [42]. Regarding the shear tab design, the AISC considers the interaction of the shear and bending moment using an elliptical interaction equation (Eq. (3)).

$$(\frac{M}{M_P}) + (\frac{P}{P_P})^2 + (\frac{(\frac{V}{V_P})^4}{1-(\frac{P}{P_P})^2}) \le 1 \tag{1}$$

$$(\frac{M}{M_P}) + (\frac{P}{P_P})^2 + (\frac{V}{V_P})^4 \le 1 \tag{2}$$

$$(\frac{M}{M_P})^2 + (\frac{V}{V_P})^2 \le 1 \tag{3}$$

The behaviour of the FE model of Specimens BG3-2-13-F-200C and BG6-2-19-F-500C was similar to the test specimens. Yielding began from the re-entrant corners of the shear plate, then propagated toward the interior bolt line. The FE models showed that the connection stiffness slightly decreased when a large portion of the shear plate along the interior bolt line yielded. The full depth of the shear plate along the net section yielded after yielding of the gross section of Specimen BG3-2-13-F-200C, while they occurred at the same time in Specimen BG6-2-19-F-

500C. Following the shear plate yielding, its out-of-plane deformation increased. Furthermore, the FE models demonstrated that the net section fracture would determine the connection's ultimate strength in the absence of beam binding. Referring to Fig. 17, the maximum plastic strain developed at the bottom re-entrant corner and at the bolt holes of the plate's upper portion.

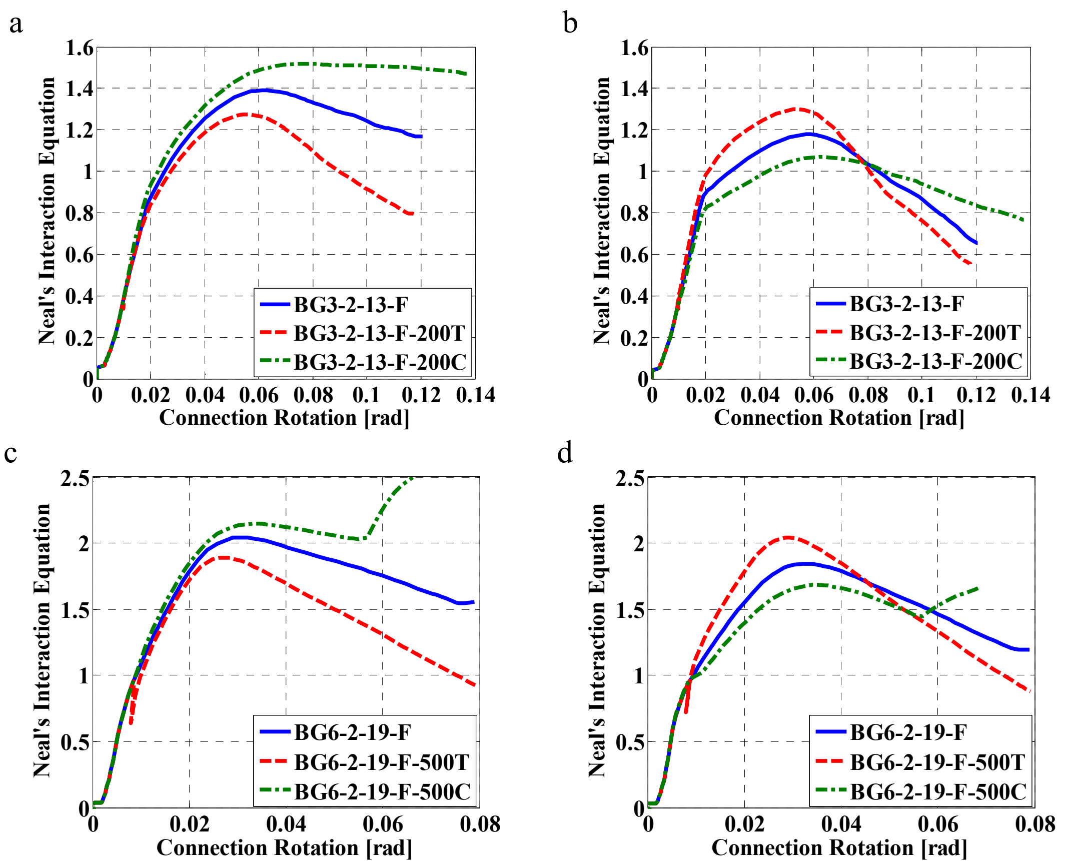

Fig. 16. Neal Interaction equation (Eq. (1)) at: (a and b) gross and net sections of Specimen BG3-2-13-F, respectively, (c and d) gross and net sections of Specimen BG6-2-19-F, respectively

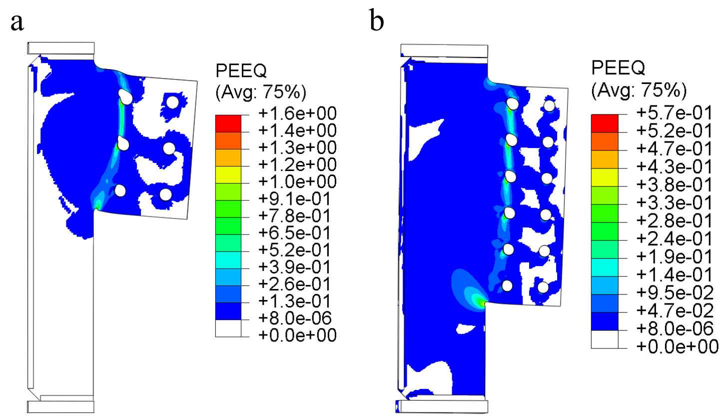

Fig. 17. Shear plate plastic strain corresponding to the net section fracture at: (a) BG3-2-1-13-F-200C, (b) BG6-2-1-9-F-500C

4.2 Shear plate internal forces along the interior bolt line

Figures 14 and 15 show that the net section, the section along the bolt line centerline, was subjected to only a portion of the connection shear force. Furthermore, applying the axial force changed the shear demand at the net section (Figs. 14b & 15b). To clarify this fact, the net shear and axial forces were compared with corresponding values from the gross section of the plate, Fig. 18. Referring to Figs. 18a and 18b, the tensile force increased the ratio between the shear force at the net and gross sections, while the compression force decreased it. Referring to Figs. 18c and 18d, the axial force along the net section was compared with the applied axial force (P_a), 200 kN and 500 kN for Specimens BG3-2-13-F and BG6-2-19-F, respectively. In comparison to the tensile force, the net section was subjected to a smaller portion of the applied axial force in the presence of the compression force. Furthermore, Figs. 18c and 18d show that the tensile force was developed along the net section even under gravity-induced shear force.

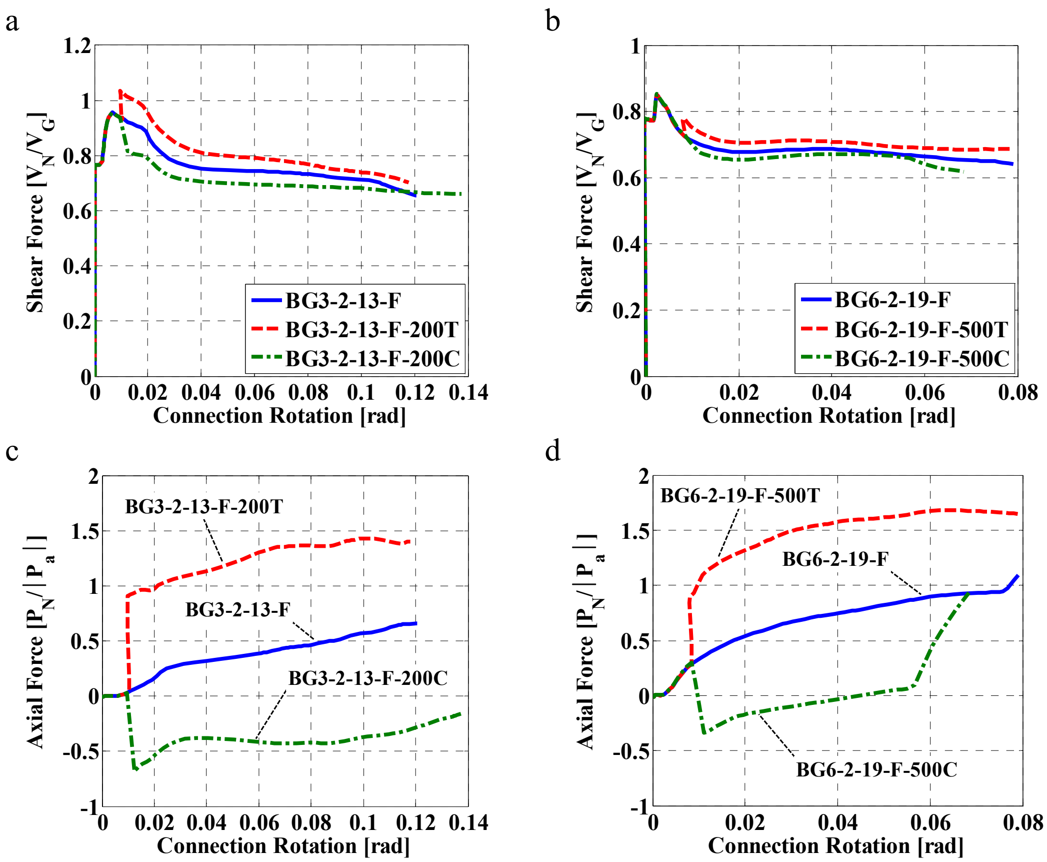

Fig. 18. FE model predictions for: (a) shear force of BG3-2-13-F models, (b) shear force of BG6-2-19-F models, (c) Axial force of BG3-2-13-F models,(d) Axial force of BG6-2-19-F models

The bearing mechanism between the bolt shanks and the bolt holes was thoroughly studied to explain the reasons for the aforementioned observations. Figure 19a shows the bolt group, which was subjected to the eccentric shear force. In addition to the vertical shear force, a horizontal force was developed in the top and bottom bolts due to the eccentric shear force and its consequent bending moment. Referring to Fig 19b, the horizontal force moved the top bolt away from the centerline of the bolt hole, while the bottom bolt moved closer to the support.

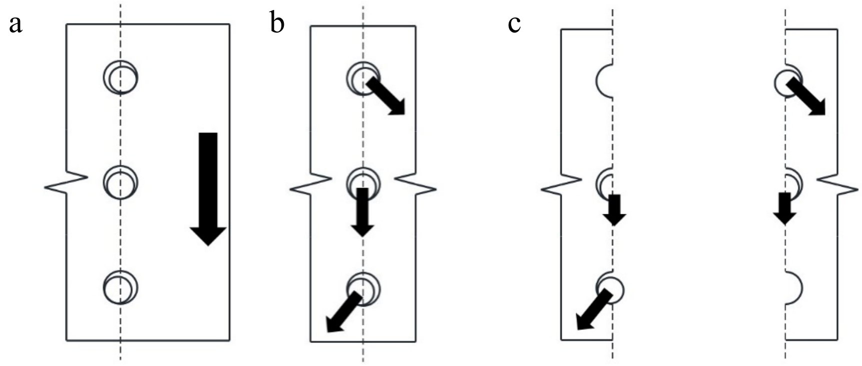

Fig. 19. Bolt group under an eccentric shear force, (a) applied shear force, (b) resultant force at each bolt

The middle bolt (Fig. 20a) transferred a shear force to the plate while it was placed along the centerline of the bolt hole. Therefore, half of the bolts' shear force was transferred through the net section. In the presence of the tensile force (the top bolt), the net section was subjected to a larger portion of the shear and axial forces as the bolt moved away from the support and crossed the bolt line centerline (Fig. 20b). Therefore, the horizontal force of the top bolt subjected the net section to the tensile force (Fig. 19c). That was the reason behind development of an extra tension in Figs. 18c and 18d. In contrast, compression pushed the bottom bolt toward the support (Fig. 20c) and the net section resisted a smaller component of the shear and axial force.

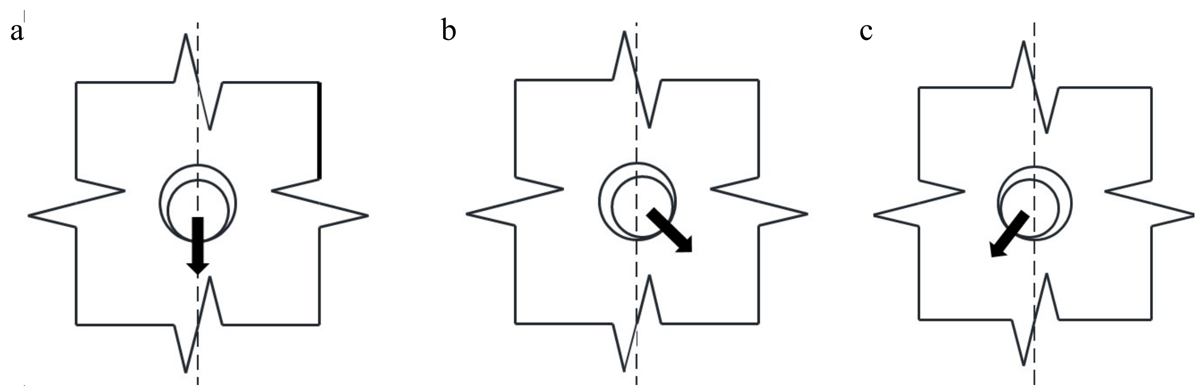

Fig. 20. Bolt under: (a) shear force, (b) shear and tension, (c) shear and compression

4.3 Effect of axial force

Referring to Figs. 14a and 15a, the axial tensile force decreased the ultimate shear resistance of the connection, while the axial compression force increased it. This occurred because the tensile force increased the force demands on the interior bolt line of the shear plate, while the compression force decreased those demands (Figs. 14b and 15b). Then, the tensile force hastened the onset of the connection's ultimate failure mode, i.e. net section fracture of the shear plate, while the axial compression force delayed the onset of this failure mode. The same observations held true for the connection resistance corresponding to the net section yielding. Referring to Table 4, the tension force caused the net section yielding to precede the gross section yielding. However, the difference between the yielding strength of the net and gross sections was small; hence, the connection could still resist much larger shear after the gross section yielding. In addition to the axial force, the ratio between the gross and net section areas affected the yielding sequence of the gross and net sections. In model BG3-2-13-F, the net section yielded shortly after the gross section, while they occurred at the same time in the BG6-2-19-F model. The aforementioned ratio, A_{net}/A_g, was equal to 0.73 and 0.69 for Specimens BG3-2-13-F and BG6-2-19-F, respectively.

Table 4. FE model predictions for connection resistance

	BG3-2-13-F			BG6-2-19-F		
Axial Load	200C	0	200T	500C	0	500T
Failure mode	Measured strength (kN)	Measured strength (kN)	Measured strength (kN)	Measured strength (kN)	Measured strength (kN)	Measured strength (kN)
Gross section yielding	507	518	517	1674	1676	1631
Net section yielding	631	545	450	1767	1676	1544
Out-of-plane deformation	662	---	---	1995	2021	---
Net section fracture	688	666	634	2120	2103	2046

Referring to Figs 14f and 15f, the axial compression force increased the plate's out-of-plane deformation, while the tension force decreased it. This observation suggested that the compression could trigger the shear plate buckling and change the connection’s ultimate failure mode, especially in the case of a slender shear plate or larger compressive force.

4.4 Evaluation of the current design procedure of extended shear tab connections

Various failure modes were observed in the studied connection configurations, both tested and numerical, including the gross and net section yielding of the shear plate, the shear plate out-of-plane deformation, and the net section fracture. Of note, the shear plate yielded at its gross and net sections because of the interaction of moment, shear and axial force. Referring to Table 5, to evaluate the accuracy of the current AISC design method [2], the results obtained from it were compared with those determined from the experimental measurements and the FE model. The design method became more accurate if the geometric eccentricity was replaced with the measured eccentricity corresponding to the gross section yielding of the shear plate. Furthermore, the current design method correctly predicted the governing failure mode when the measured eccentricity was implemented. Referring to Table 5, although the AISC elliptical moment-shear interaction equation (Eq. (3)) resulted in a conservative estimate of the moment-shear-axial force yielding of the shear plate gross section, it might overestimate the shear plate yielding strength in the presence of a large axial force. Based on Eqs. (1) and (2), the shear plate gross section of Specimens BG3-2-13-F-200C and BG6-2-19-F-500C yielded at a connection shear force equal to 496 kN and 1595 kN, respectively. Furthermore, the current design procedure might significantly overestimate the buckling strength of Specimen BG6-2-19-F-500C, because it neglected the detrimental effects of the axial and shear forces on the plate’s flexural capacity. To address this issue, Dowswell & Whyte [27] used Eq. (1) to determine the available flexural buckling strength in the presence of the shear and axial forces. If this advice was taken for the test specimens, the buckling strength of the extended portion of the shear plate was equal to the applied force corresponding to the gross section yielding of the shear plate. To calculate the weld group capacity under an eccentric shear force, the Instantaneous Centre of Rotation (ICR) method was implemented for the C-Shape weld group, while only the vertical weld lines were considered in the calculation of the weld group capacity under a concentric shear force.

Table 5. Connection resistance to different failure modes

	BG3-2-13-F-200C			BG6-2-19-F-500C		
Failure mode	Expected strength[1] (kN)	Expected strength[2] (kN)	Measured strength (kN)	Expected strength[1] (kN)	Expected strength[2] (kN)	Measured strength (kN)
Plate moment-shear-axial force yielding	391	482[3]	507	1251	1630[3]	1674
Plate Shear yielding	761	761	--	1976	1976	1976
Bolt bearing	377	978	--[4]	1771	4202	--[4]
Plate buckling	456	625[5]	662[6]	1616	2885[5]	1995[6]
Rupture at net section of shear plate	648	648	687	1824	1824	2120
Bolt shear	337	874	>687	1169	2774	>2120
Weld tearing	2524	2334[7]	--	4451	4777[7]	--

[1] Expected strength based on geometric eccentricity (e)
[2] Expected strength based on measured eccentricity
[3] Yielding strength of the extended portion of the shear plate based on elliptical yield criterion (Eq. (3))
[4] Although large bearing deformation was observed, bearing failure did not occur
[5] Buckling strength of the extended portion of the shear plate
[6] Shear resistance corresponding to the shear plate out-of-plane deformation
[7] Strength of C-shape weld group

Among the observed failure modes, the gross section yielding of the shear plate occurred earlier under a smaller shear force. Furthermore, other failure modes occurred when the connection underwent large deformation and rotation, which negatively affected the supported beam's serviceability. Therefore, the moment-shear-axial force yielding of the shear plate's gross section should be considered as a conservative estimate of the connection's capacity. In the presence of the axial tensile force, yielding of the net section preceded yielding of the gross section (i.e. BG3-2-13-F-200T and BG6-2-19-F-500T). However, the yield strength of the gross section was still a conservative estimate of the connection's capacity because the difference between the yield strength of the gross and net sections was small and the connection was able to resist a much larger shear force.

5 Conclusions

Two full-scale specimens were tested in order to deepen our understanding of the behaviour of the double-sided configuration of the full-depth extended beam-to-girder shear tab under coupled gravity and axial force demands. The test specimens were constructed of different features, including shear plate dimensions, bolt size, bolt group configuration, geometric eccentricity, beam and girder sizes. Furthermore, validated finite element models were adopted to investigate the dependency of the connection's behaviour on critical parameters including the axial force direction and the force distribution along the plate net section. The main findings of the paper are summarized as follows:

- The double-sided configuration of the full-depth extended beam-to-girder shear tab yielded through its net section along the bolt line, the closest to the girder. Furthermore, the gross section yielding of the shear plate occurred along the outer end of its re-entrant corners.
- The net section fracture was determined as the ultimate failure mode of the studied connections.
- The net section along the centerline of the plate's interior bolt line was subjected to a portion of the connection axial and shear forces. This amount depended on the number of vertical bolt lines, bolt hole diameter, the distance between bolt holes, the axial load direction and magnitude, and the initial position of the bolt in its hole.

- The compressive axial load increased the out-of-plane deformation of the shear plate, which could result into plate buckling in the case of the slender shear plate or a larger compression force. The axial compression force decreased the shear force demand on the net section.
- The tensile axial force accelerated the plate yielding and fracture along the interior bolt line by increasing the force demands on the shear plate's net section. Furthermore, the tensile force decreased the shear plate's out-of-plane deformation and delayed the plate buckling.
- The gross section yielding strength of the shear plate could be considered as a conservative estimate of the connection capacity as the connection resisted much larger shear force following the gross section yielding of the shear plate. Further analyses are needed to validate this finding in the presence of a large tensile force.
- The current design method significantly underestimated the connection shear capacity due to the assumption that the inflection point formed at the girder web's face. In contrast, the inflection point formed far away from the girder web, farther from the bolt group centroid.

6 Acknowledgments

The authors would like to thank the ADF Group Inc. and DPHV Structural Consultants for their generous technical and financial support, as well as the Natural Sciences and Engineering Research Council of Canada. The finite element computations were conducted on the McGill University supercomputer Guillimin, which is managed by Calcul Québec and Compute Canada. The supercomputer operation is funded by the Canada Foundation for Innovation (CFI), NanoQuébec, RMGA and the Fonds de recherche du Québec - Nature et technologies (FRQ-NT).

7 References

[1] AISC 360-16, Specification for structural steel buildings, American Institute of steel Construction, Chicago, IL, 2016.

[2] AISC 325-17, Steel construction manual, 15th edition, American Institute of steel Construction, Chicago, IL, 2017.

[3] K. Thomas, Design and behaviour of extended shear tabs under combined loads, Master Thesis, University of Alberta, Edmonton, Alberta., 2014.

[4] A.R. Tamboli, Handbook of structural steel connection design and details, Third edition, McGraw-Hill, New York, NY., 2016.

[5] CSA-S16-14, Design of steel structures, Canadian Standards Association, Mississauga, ON., 2014.

[6] D.R. Sherman, A. Ghorbanpoor, Design of extended shear tabs, University of Wisconsin-Milwaukee, Milwaukee, WI, 2002.

[7] J. Hertz, Testing of extended shear tab connections subjected to shear, Master's Thesis, McGill University, Montreal, QC, 2014.

[8] N. Goldstein Apt, Testing of extended shear tab and coped beam-to-girder connections subject to shear loading, Master's Thesis, McGill University, Montreal, QC, 2015.

[9] M. Motallebi, D.G. Lignos, C.A. Rogers, Behavior of stiffened extended shear tab connections under gravity induced shear force., J. Constr. Steel Res., Under Review (2018).

[10] M. Motallebi, D.G. Lignos, C.A. Rogers, Stability of stiffened extended shear tab connections under gravity induced shear force, J. Constr. Steel Res., Under Review (2018).

[11] W. Goodrich, Behavior of extended shear tabs in stiffened beam-to-column web connections, Thesis, Vanderbilt University, Nashville, TN, 2005.

[12] K. Thomas, R.G. Driver, S.A. Oosterhof, L. Callele, Full-scale tests of stabilized and unstabilized extended single-plate connections, Structures, 10 (2017) 49-58.

[13] M. Marosi, Behaviour of single and double row bolted shear tab connections and weld retrofits, Master's Thesis, McGill University, Montreal, QC, 2011.

[14] M. Marosi, M. D'Aronco, R. Tremblay, C.A. Rogers, Multi-row bolted beam to column shear tab connections, 6th European Conference on Steel and Composite Structures, Budapest,Hungary, 2011.

[15] M. D'Aronco, Behaviour of double and triple vertical rows of bolts shear tab connections and weld retrofits, Master's Thesis, École Polytechnique de Montréal, Montreal, QC, 2013.

[16] A. Mirzaei, Steel shear tab connections subjected to combined shear and axial forces, PhD Thesis, McGill University, Montreal, QC, 2014.

[17] J. Hertz, D.G. Lignos, C.A. Rogers, Full scale testing of extended beam-to-column and beam to-girder shear tab connections subjected to shear, 8th International Conference on Behavior of Steel Structures in Seismic Areas, Shanghai, China, 2015.

[18] C.A. Rogers, M. Marosi, J. Hertz, D.G. Lignos, R. Tremblay, M. D'Aronco, Performance of weld-retrofit beam-to-column shear tab connections, 8th Int. Workshop on Connections in Steel Structures, Boston, MA., 2016.

[19] ASTM A992 / A992M-11(2015), Standard specification for structural steel shapes, ASTM International, West Conshohocken, PA, 2015.

[20] ASTM A572 / A572M-15, Standard specification for high-strength low-alloy columbium-vanadium structural steel, ASTM International, West Conshohocken, PA, 2015.

[21] ASTM F3125 / F3125M-15a, Standard specification for high strength structural bolts, steel and alloy steel, heat treated, 120 ksi (830 mpa) and 150 ksi (1040 mpa) minimum tensile strength, inch and metric dimensions, ASTM International, West Conshohocken, PA, 2015.

[22] ASTM A370-17, Standard test methods and definitions for mechanical testing of steel products, ASTM International, West Conshohocken, PA, 2017.

[23] AWS A5.20/A5.20M:2005 (R2015), Carbon steel electrodes for flux cored arc welding, American Welding Society, Miami, FL., 2015.

[24] A.M. Kanvinde, I.R. Gomez, M. Roberts, B.V. Fell, G.Y. Grondin, Strength and ductility of fillet welds with transverse root notch, J. Constr. Steel Res., 65 (2009) 11.

[25] AISC 341-16, Seismic provisions for structural steel buildings, American Institute of steel Construction, Chicago, IL, 2016.

[26] AISC 325-11, Steel construction manual, 14th edition, American Institute of steel Construction, Chicago, IL, 2011.

[27] B. Dowswell, R. Whyte, Local stability of double-coped beams, Eng. J. AISC, 51(1) (2014) 43-52.

[28] J.-J. Cheng, J. Yura, C. Johnson, Design and behavior of coped beams, University of Texas at Austin, Austin, TX, 1984.

[29] L. Muir, W. Thornton, A direct method for obtaining the plate buckling coefficient for double-coped beams, Eng. J. AISC, 41 (2004) 133-134.

[30] L.S. Muir, C.M. Hewitt, Design of unstiffened extended single-plate shear connections, Eng. J. AISC, 46(2) (2009) 67-80.

[31] A. Astaneh, K.M. McMullin, S.M. Call, Behavior and design of steel single plate shear connections, J. Struct. Eng. ASCE, 119(8) (1993) 2421-2440.

[32] A. Astaneh, Demand and supply of ductility in steel shear connections, J. Constr. Steel Res., 14(1) (1989) 1-19.

[33] ABAQUS 6.11-3, [Computer software], Dassault Systemes Simulia Corp., Providence, RI.

[34] G.L. Kulak, J.W. Fisher, J.H. Struik, Guide to design criteria for bolted and riveted joints, AISC, Chicago,IL, 2001.

[35] ASTM A6 /A6M, General requirements for rolled structural steel bars, plates, shapes, and sheet piling, ASTM International, 2004.

[36] CSA-G40.20-13/G40.21-13, General requirements for rolled or welded structural quality steel/ structural quality steel, Canadian Standards Association, Toronto, ON., 2013.

[37] CISC, Handbook of steel construction, Canadian Institute of Steel Construction, Markham, ON., 2016.

[38] A. Elkady, D.G. Lignos, Analytical investigation of the cyclic behavior and plastic hinge formation in deep wide-flange steel beam-columns, Bull. Earthq. Eng., 13(4) (2015) 1097-1118.

[39] B.A. Mohr, T.M. Murray, Bending strength of steel bracket and splice plates, Eng. J. AISC, 45(2) (2008) 97-106.

[40] P. Salem, Unified design criteria for steel cantilever plate connection elements, PhD Thesis, University of Alberta, Edmonton, AL., 2016.

[41] B.G. Neal, The effect of shear and normal forces on the fully plastic moment of a beam of rectangular cross section, Journal of Applied Mechanics, 28(2) (1961) 269-274.

[42] A. Astaneh, Seismic behavior and design of gusset plates, Steel Tips, Structural Steel Education Council, Moraga, CA., 1998.